Published in final edited form as:
J Proteome Res. 2010 March 5; 9(3): 1510–1521. doi:10.1021/pr901022m.

Proteomic identification of Hsc70 as a mediator of RGS9-2 degradation by *in vivo* interactome analysis

Ekaterina Posokhova[1], **Vladimir Uversky**[2,3], and **Kirill A. Martemyanov**[1]

[1]Department of Pharmacology, University of Minnesota, Minneapolis, MN 55455

[2]Institute for Intrinsically Disordered Protein Research,Department of Biochemistry and Molecular Biology, Indiana University School of Medicine, Indiana, IN 46202 USA

[3]Institute for Biological Instrumentation, Russian Academy of Sciences, 142290 Pushchino, Moscow Region, Russia

Abstract

Changes in interactions between signaling proteins underlie many cellular functions. In the mammalian nervous system a member of the Regulator of G protein Signaling family, RGS9-2 (Regulator of G protein Signaling, type 9) is a key regulator of dopamine and opioid signaling pathways that mediate motor control and reward behavior. Dynamic association of RGS9-2 with a neuronal protein R7BP (R7 family Binding Protein) has been found to be critically important for the regulation of the expression level of the complex by proteolytic mechanisms. Changes in RGS9-2 expression are observed in response to a number of signaling events and are thought to contribute to the plasticity of the neurotransmitter action. In this study, we report an identification of molecular chaperone Hsc70 (Heat shock cognate protein 70) as a critical mediator of RGS9-2 expression that is specifically recruited to the intrinsically disordered C-terminal domain of RGS9-2 following its dissociation from R7BP. Hsc70 was identified by a novel application of the quantitative proteomics approach developed to monitor interactome dynamics in mice using a set of controls contributed by knockout strains. We propose this application to be a useful tool for studying the dynamics of protein assemblies in complex models, such as signaling in the mammalian nervous system.

Keywords

Regulator of G protein Signaling; heat-shock proteins; protein degradation; neuronal signaling; quantitative proteomics; protein-protein interactions; basal ganglia; drug addiction

INTRODUCTION

Assembly of proteins into macromolecular complexes is a fundamental property that underlies a vast number of cellular signaling reactions involving ion channels, transcriptional machinery and receptor signaling pathways. Individual subunits often contribute unique properties making re-arrangement of the complex composition a powerful mechanism for the regulation of cellular responses. Cells, in turn, tightly regulate the assembly, composition and interaction stoichiometries within these complexes by an array of mechanisms. Controlled protein degradation is one of the central mechanisms that allow rapid changes in the makeup of macromolecular complexes and thus determines their functional dynamics in cells.

Address correspondence to: Dr. Kirill Martemyanov, 6-120 Jackson Hall, 321 Church Street S.E. Minneapolis, MN 55455. Fax: (612) 625-8408, martemyanov@umn.edu.

Multi-subunit organization shaped by proteolysis is a consistent theme in the regulation of G protein signaling in the nervous system by the members of the R7 family of RGS (Regulator of G protein signaling) proteins [1]. R7 RGS proteins act to accelerate the inactivation of G protein signaling by stimulating the rate of the GTP hydrolysis on the alpha subunits of heterotrimeric G proteins thus speeding up termination of the cellular response following GPCR activation. The best studied member of the R7 RGS proteins, RGS9-2, is selectively enriched in the striatum region of the brain and has been demonstrated to play critical roles in controlling nociception, locomotion and reward behavior by controlling the activity of μ-opioid and dopamine receptor signaling (See[1-3] for recent reviews). RGS9-2 forms trimeric complex with its two other subunits, the type 5 G protein beta subunit (Gβ5) [4-6] and the SNARE-like R7 Binding Protein (R7BP) [5, 7]. Association with Gβ5 is strictly required for the expression of RGS9-2, as well for all other R7 RGS proteins, and genetic knockout of Gβ5 in mice results in the elimination of R7 RGS proteins [6]. Similarly, association with R7BP is also required for achieving a high expression level of RGS9-2 in the striatum[8] and elimination of R7BP in mice makes RGS9-2 susceptible to degradation by cellular cysteine proteases substantially reducing its levels [9]. However, in contrast to Gβ5 elimination, R7BP knockout does not affect the expression of other R7 RGS proteins and leaves readily detectable amounts of RGS9-2 [9] suggesting that association with R7BP serves as regulatory mechanism that selectively modulates the abundance of the RGS9-2/Gβ5 complex. Indeed, changes in neuronal activity and oxygenation status were found to reduce RGS9-2 expression concomitant with the decrease in RGS9-2/Gβ5 coupling to R7BP [10], while viral-mediated over-expression of R7BP results in the elevation of RGS9-2 levels [9]. Furthermore, RGS9-2 expression in the striatum is uniquely sensitive to the administration of psychostimulants and morphine [11-13] which is believed to be an important feedback mechanism underlying adaptations in the striatum upon the development of drug addiction [3]. Together, these findings suggest that the dynamic coupling/un-coupling of RGS9-2/Gβ5 with R7BP serves as a critical regulatory event that determines the abundance of this signaling regulator by post-translational mechanisms involving protein degradation. What remains unknown however are the molecular details of processes that control and/or mediate RGS9-2/Gβ5 degradation.

In this study we report the identification of molecular interactions that underlie RGS9-2/Gβ5 instability upon dissociation of R7BP from the complex. We have developed an iTRAQ®-based proteomics approach that allows quantification of changes in the composition of protein complexes induced by genetic manipulations in mice. This method was applied to identify the interactions of RGS9-2/Gβ5 complex that are up-regulated in the striatum of the R7BP knockout mouse. Based on the changes in the interactome we detected, we propose a model of molecular events controlling RGS9-2 degradation where the key role is played by molecular chaperone Hsc70.

EXPERIMENTAL PROCEDURES

Antibodies, Recombinant Proteins, DNA Constructs and Mouse Strains

Generation of sheep anti-R7BP (N-terminal epitope) and sheep anti-RGS9-2CT (C-terminal epitope) has been described previously [5]. Antibodies were affinity purified and stored in PBS buffer containing 50% glycerol. Rabbit anti-Gβ5 (SGS) antibodies were a generous gift from Dr. William Simonds, NIDDK. Rat monoclonal anti-Hsc-70 (clone 1B5) antibodies were from Assay Designs (Ann Arbor, MI). Mouse monoclonal anti-β-actin (clone AC-15) antibodies were purchased from Sigma (St. Louis, MO). Mouse monoclonal anti-c-myc (clone 9E10) antibodies were from Roche Applied Sciences (Indianapolis, IN). The Anti-HA tag antibody was a mouse monoclonal from Millipore (Temecula, CA). All general chemicals were purchased from Sigma Aldrich.

The recombinant C-terminus of RGS9-2 protein was purified from Sf9 cells. The DNA region encoding amino acids 467-675 of mouse RGS9-2 was appended at the 5'end with the his-tag encoding sequence by PCR and cloned into a baculovirus shuttle vector, pVL1392, that was used to generate recombinant baculovirus. A high titer baculoviral stock was applied to 2 liters of Sf9 cell culture at MOI=3. Following 3 days of post-infection incubation, cell were collected, disrupted in lysis buffer (20 mM Tris-HCl, pH=8.0, 150 mM NaCl supplemented with Complete (Roche) protease inhibitors and the recombinant C-terminus was purified on Ni-NTA beads as described previously [14]. Protein quantification was performed using Bradford reagent (Sigma) according to the manufacture's specifications using BSA as a standard (Pierce).

Cloning of full length R7BP, Gβ5, RGS9-2 was described previously [5, 15]. For expression in mammalian cells, the HA-tag was added at the 5'-end of the RGS9-2 C-terminus (aa 467-675) by PCR and the cassette was cloned into the pcDNA3.1 vector between EcoRI and Not restriction sites. The rat N-terminal myc-tagged Hsc70 construct was a generous gift from Dr. Cam Patterson, UNC, and it was further subcloned into the pcDNA3.1/V5-His-TOPO (Invitrogen) mammalian expression vector according to the manufacture's specifications. The HA-tagged N-terminus (aa 1-209) of the RGS9 protein was cloned into the pcDNA3.1/V5-His-TOPO (Invitrogen) mammalian expression vector according to the manufacture's specifications. All constructs were propagated using an E.coli Top-10 strain (Invitrogen), isolated using Maxiprep kits (Qiagen) and sequenced.

The generation of the R7BP knockout has been described previously [9]. RGS9 knockout mice [16] have been generously provided by Dr. Jason Chen (Virginia Commonwealth University). Mice were housed in groups on a 12h light/dark cycle with food and water available *ad libitum.* All procedures were carried out in accordance with the National Institute of Health guidelines and were granted formal approval by the Institutional Animal Care and Use Committee of the University of Minnesota.

Preparative immunoprecipitation of RGS9-2 complexes from mouse striatum

For the preparation of brain lysates, punches of striatal tissue were dissected from mouse brains immediately upon sacrificing. Tissue was homogenized in immunoprecipitation (IP) buffer composed of PBS (pH=7.4, ThermoFisherScientific) supplemented with an additional 150 mM NaCl, 1% Triton X-100, Complete protease inhibitors (Roche) and Phosphatase Inhibitor Cocktails I and II (Sigma) by passing it through a series of needles decreasing in gauge. Following a 30 minute incubation at 4°C, insoluble material was removed by centrifugation at 200,000 × g for 15 minutes. Supernatants were incubated for 1 hour at 4^0C with 50 μg of anti-RGS9-2 CT antibody covalently coupled to 10 μl of protein G beads (GE Healthcare) with Bis (Sulfosuccinimidyl)suberate (BS3) (Pierce) as described previously [5]. The beads were washed three times with ice-cold IP buffer and proteins were eluted with 200 μl of 5% NH_4OH, lyophilized using a SpeedVac concentrator, and processed for mass-spectrometric analysis as described in the following sections.

Pull-down of brain proteins with recombinant C-terminus of RGS9-2

Whole brain extract from wild-type mice was prepared by homogenizing the tissue in pull-down (PD) buffer (1xPBS, 150 mM NaCl, 0.1% n-Dodecanoylsucrose and protease inhibitors) in a glass homogenizer and passing the suspension through a series of needles with varying gauge sizes. Following a 30 minute incubation at 4°C, the lysate was centrifuged for 15 minutes at 14,000 × g. The supernatant was incubated for 90 minutes at 4°C with 20 μl beads covalently bound to 35 μg of recombinant RGS9-2 C-terminus by SulfoLink kit (Pierce) according to the manufacturer's protocol, except that all coupling procedures were performed in 20 mM Tris, pH 7.8 supplemented with 300 mM NaCl, 10% glycerol and protease inhibitors. Non-conjugated beads were used as a negative control. Following incubation, beads were washed

3 times with the PD buffer, bound proteins were eluted with 5% NH_4OH, lyophilized using a SpeedVac concentrator, and processed for mass-spectrometric analysis as described in the following sections.

iTRAQ® labeling and preparation of samples for mass-spectometry

Samples from preparative IP were dissolved in 0.5 M triethylammonium bicarbonate (pH 8.5) containing 0.1% SDS, reduced with 5mM tris-(2-carboxyethyl) phosphine for 1hr at 60C and alkylated with 10 mM methyl methanethiosulfonate for 10 minutes at room temperature. Proteins were digested with 10 μg of modified porcine trypsin (Promega) at 37°C for 16 hrs. iTRAQ® labeling reagents (Applied Biosystems) were reconstituted in ethanol, added to tryptic digests (wild-type, iTRAQ® 114; R7BP knockout, iTRAQ® 115; RGS9 knockout, iTRAQ® 116) and incubated at room temperature for 1 hr. Differentially labeled peptide mixtures were combined and dried out in a SpeedVac. In some experiments iTRAQ® 116 labeled samples (RGS9 -/-) were not mixed with other samples and were processed separately. Labeled peptide mixtures were reconstituted in 0.2% formic acid (Pierce) and applied to an MCX cartridge (Waters) pre-equilibrated with methanol/water (1:1, vol/vol). The cartridge was washed with 0.1% formic acid in 5% methanol followed by a 100% methanol wash. Peptides were eluted from MCX resin in 1 ml of 1.5% NH_4OH in methanol, dried by SpeedVac and subjected to separation by liquid chromatography as described below.

Samples from pull-down experiments were dissolved in 20 μl of SDS sample buffer (62mM Tris, 10% glycerol, 2%SDS, 5% β-ME), and resolved by SDS-PAGE (Lonza). Gels were fixed with 5% acetic acid in 50% methanol for 20 minutes and stained with NOVEX Colloidal Blue staining kit (Invitrogen) overnight. Band(s) present in RGS9-2 C-terminus pull-down sample were cut out with a razor blade. A corresponding piece of gel of a matching molecular weight was also excised from the control sample where empty beads were used for the pull-down. In-gel digestion with porcine sequencing grade modified trypsin (Promega) was performed following sample reduction, alkylation and destaining as described previously [17]. Final samples were dissolved in 10 μl of 0.1% trifluoroacetic acid (TFA) in 50% acetonitrile (ACN) and 0.7 μl of each sample was mixed with an equal amount of 6 mg/mL α-cyano-4-hydroxycinnamic acid (Fluka) in an ACN:H_2O mixture (75:25 v/v), 0.1% TFA, 10 mM ammonium phosphate and spotted on a MALDI target in 384-spot format.

Liquid Chromatography and MALDI mass-spectromerty

The Tempo™ LC MALDI spotting system (ABI) was used to separate iTRAQ®-labeled peptides and deposit LC eluates into fractions robotically spotted onto LC MALDI targets in a 1232-spot format. Peptides were dissolved in 0.1% formic acid in a 98:2 ratio, water:ACN mixture, loaded onto a ProteoCol™ C18 trap cartridge (SGE Analytical Science, Victoria, Australia: 300 Å pore size, 300 μm internal diameter, 10 mm length). The cartridge was washed with a loading buffer for 18 minutes at 9 μl/min with loading buffer and then connected to a C18 analytical column made of ~12 cm of 100 μm Integrafrit™ tubings (New Objective, Woburn, MA) packaged with Magic 5 μm 200 Å C18AQ (Michrom BioResources, Auburn, CA). Peptides were eluted at 500 nl/min flow rate by gradually increasing the ratio of elution buffer (98:2, ACN:water, 0.1% TFA) to the starting buffer (98:2, water:ACN, 0.1% TFA) according to the following profile. From 0 to 5 min concentration of elution buffer increased to 15%, by 52 min to 35%, by 54 min to 80% at which point it was held constant at an 80% level for 10 minutes. Peptide elution was monitored by UV absorbance at 214 nm. Eluted fractions were mixed prior to spot deposition with a matrix solution (6 mg/mL alpha-cyano-4-hydroxycinnamic acid) at a rate of 1 μl/min using a Harvard Apparatus (Holliston, MA) syringe pump and deposited in 24 second intervals.

All mass-spectrometric data were acquired on a 4800 MALDI TOF/TOF™ analyzer (ABI) with a 200 Hz repetition rate Nd:YAG laser. TOF MS spectra were acquired from 800 – 4000 *m*/z. A total of 800 to 1000 laser pulses were accumulated for each TOF MS spectrum fixed laser setting following an optimization protocol. Tandem MS mode was operated with 2kV collision energy with CID gas (air) over a range of 10 *m/z* to 95% of the precursor mass value. Precursor mass window was 250 ppm (FWHM) in relative mode. A minimum of 800 and a maximum of 4000 laser shots were accumulated with laser stop conditions set at 6 product ion peaks of S/N > 60 and an optimized, fixed laser setting. The metastable suppressor setting was on. Data dependent tandem MS settings included acquisition of the top 10 most intense ion signals per spot (top 25 for gel-derived samples). In the cases where 2 or more consecutive spots in an LC run showed identical precursor *m/z* values (within 200 ppm tolerance), tandem MS was acquired exclusively from the spot with the maximum S/N (signal to noise ratio), as determined from the TOF MS spectra.

Database searches and MS data analysis

Tandem mass spectra were searched using ProteinPilot™ 2.0.1 software, revision number 67476 (Applied Biosystems, Inc.) with the ParagonTM search algorithm against the National Center for Biotechnology Information's Reference Sequence mouse subset protein database (ver. 11-01-07; http://www.ncbi.nlm.nih.gov/), which contained 34,715 proteins including 179 contaminant proteins from Thermo Scientific. Parameters for preparative IP samples were “iTRAQ® 4plex (peptide labeled)” sample type, MMTS-cysteine modifications, trypsin digest, thorough search with biological modifications ID focus, and 66% protein confidence threshold. Search parameters for pull-down samples were the same except for sample type (“gel-based ID”) and cysteine modifications (iodoacetomide). Protein identifications with at least 95% confidence as determined by ProteinPilot software were considered significant.

In each separate quantification experiment, the ratio for all proteins was normalized to the 115:114 of RGS9-2. To perform the normalization, manual bias correction was applied to 115/114 iTRAQ® ratios. The manual bias correction was calculated from the product of the 115/114 value for RGS9-2 and the auto-bias value provided by ProteinPilot™ software. The normalization accounted for both the difference in total sample amounts and amounts of precipitated RGS9-2. Protein summary data that included, but was not limited to, ProteinPilot scores for protein identification, percent coverage, iTRAQ® ratios and their p-values were exported from ProteinPilot as tab-delimited text with manual bias correction applied. Normalized data from both experiments was pooled together. Proteins identified from immunoprecipitations with RGS9 knockout samples were considered non-specific and excluded from the dataset. Only proteins that showed a statistically significant change in levels between wild-type and R7BP knockout samples (p-value115/114 < 0.05, EF<2) were included in the final report. The EF is a measure of how well a mean protein ratio was determined (a reflection of the variance and the number of peptide measurements), and is used to calculate the 95% confidence interval (CI) of the average *iTRAQ*® ratio for each protein [EF = 95% CI, where 95% CI range = (ratio × EF) – (ratio / EF)].

Cell culture, transfections and RNA interference

HEK293FT cells were obtained from Invitrogen and cultured at 37°C and 5% CO_2 in DMEM (Dulbecco's Modified Eagle Medium; GIBCO) supplemented with 100 units of penicillin and 100 μg of streptomycin, 10% FBS, 1x MEM non-essential amino acids (GIBCO), 1mM sodium pyruvate and 4 mM L-glutamine. Cells were transfected at ~ 70% confluency, using Lipofectamine LTX (Invitrogen) according to the manufacturer's protocol. The ratio of Lipofectamine to DNA used was 6.25 μl : 2.5 μg per 10 cm^2 cell surface. Cells were grown for 24-48 hours post-transfection. Equal amounts of each construct were transfected, balanced when necessary by empty pcDNA3.1 vector. In experiments testing the ability of C-terminus

of RGS9-2 to protect RGS9-2 from degradation, 0.25 μg RGS9-2 and 0.25 μg Gβ5 constructs were co-transfected with or without 2 μg of construct encoding C-terminus of RGS9-2.

The following siRNA duplexes were purchased from Quiagen: human HSPA8, sense (r(AAG CUG CUA UAG UAA GUU A)dTdT) and antisense (r(UAA CUU ACU AUA GCA GCU U) dAdA). siRNAs (0.4 nmol) of HSPA8 or equivalent amount of non-silencing AllStars control siRNA (Qiagen) were transfected when cells were at ~40% confluence using Lipofectamine 2000 (Invitrogen) according to the manufacturer's protocol. The ratio of Lipofectamine to siRNA used was 4 μl : 0.4 nmol per 10 cm^2 cell surface. Cells were allowed to grow for 24 hrs before transfection with RGS9-2/Gβ5 complex. Cells were collected for analysis 24 hrs following transfection with RGS9-2/Gβ5, lysed and protein expression was analyzed by quantitative Western blotting using an Odyssey infrared imager (LiCor).

Co-immunoprecipitation assays and Western blotting

Cellular or striatal lysates were prepared in IP buffer lacking phosphatase inhibitors and centrifuged for 15 minute at 14,000 × g. The resulting extracts were incubated with 3 μg of antibodies and 10 μl of protein G beads (GE Healthcare) for 1 hour at 4^0C. After 3 washes with ice-cold binding buffer proteins bound to the beads were eluted with SDS-sample buffer. Eluates were resolved on 12.5% SDS-PAGE gel, transferred onto PVDF membrane (Millipore) and subjected to Western blot analysis using HRP conjugated secondary antibodies and an ECL West Pico (Pierce) detection system. For quantification, samples were analyzed by infrared Western blotting using IRDye680 and IRDye800 labeled secondary antibodies (Li-Cor Biosciences) according to the manufacturer's protocol. Detection and quantification of specific bands was performed on an Odyssey Infrared Imaging System (Li-Cor Biosciences). The integrated intensity of each band of interest was measured in a corresponding channel with a top-bottom background setting. Integrated intensity of β-actin was used for data normalization.

Bioinformatics

Disorder predictions were done using a recently developed Various Short-Long version 2 algorithm of the Predictor Of Natural Disordered Regions (PONDR®-VSL2). This algorithm consists of an ensemble of logistic regression models that predict per-residue order-disorder [18, 19]. The predictor assigns a score ranging from 0 to 1 to each residue reflecting the likelihood for a given residue to adopt disordered conformation, with scores above the threshold of 0.5 corresponding to residues predicted to be disordered.

RESULTS

Analysis of changes in the RGS9-2 interactome in R7BP knockout mice

In order to identify proteins that differentially interact with RGS9-2 when R7BP is removed from the complex, we have developed a proteomic approach based on differential labeling with iTRAQ® reagents (Fig. 1). Although iTRAQ® has become a standard tool for quantitative proteomic analysis [20], we, for the first time to our knowledge, attempt to analyze system wide changes in the interaction network of the signaling regulator using genetic mouse knockouts. RGS9-2 was immunoprecipitated, in parallel, from striatal tissue lysates obtained from wild-type and R7BP-/- mice. In addition, precipitation from RGS9-/- tissue lysates served as a control to account for non-specific interactions. Proteins present in eluates were digested with trypsin and resulting peptides were differentially labeled with iTRAQ® reagents (Fig. 1). At this point samples were combined and peptides were separated by liquid chromatography (Fig. 2A) followed by mass-spectrometric identification of peptides by MALDI TOF/TOF (Fig. 2B). The experiment was conducted twice and the results of both experiments were reviewed together. A total of 680 unique peptides were identified, of which 519 had peptide confidence

scores ≥ 95% as determined by ProteinPilot™'s Paragon scoring algorithm [21]. Protein inference from peptide hits resulted in the identification of 134 distinct mouse proteins with ≥66% confidence threshold as defined by ProteinPilot™ software, which proportionally weighs contributions of individual peptide scores to the protein identification confidence. iTRAQ® label was present on more than 96% of identified peptides. A typical MS/MS spectrum acquired on the TOF/TOF and used for quantification is presented in Fig 2C. Fragmentation of the peptide $_{iTQ}$DMQNPETGVR from RGS9-2 protein (Fig 2C, *insert*) showed strong iTRAQ® reporter ion signals with signal intensity variation that was consistent with changes in RGS9-2 expression levels in different samples as determined by Western blotting (Fig. 3B). Comparison of iTRAQ® reporter ion signal intensities (114/115) revealed 4.85-fold ($p<0.001$) difference in the abundance of RGS9-2 present in the wild-type as compared to R7BP-/- samples (Fig 3A). This is in a good agreement with a 3.5±0.2-fold difference ($p<0.001$) detected by quantification of the Western blotting data (Fig 3B). In addition to RGS9-2, we readily detected its known interaction partners, R7BP and Gβ5 by both Western blotting and mass-spectometry (Fig. 3A,B). Furthermore, decrease in levels of RGS9-2 in R7BP-/- samples resulted in a similar decrease in amount of co-precipitated Gβ5 as measured by iTRAQ® technology (115/114 ratio of 0.313 vs. 0.206, Fig 3A). This result is consistent with previously reported quantification of the Western blotting data [9] and indicates unchanged stoichiometry of RGS9-2 interaction with Gβ5, upon the removal of R7BP from the complex.

Mass spectrometric signals from the 116 reporter ions from RGS9-2 peptides were substantially reduced (116/114 ratio of 0.162, $p=3.01\times10^{-20}$; Fig. 3A), but did not disappear completely as would be expected given the absence of RGS9-2 in RGS9-/- samples. Similar observations were made with 115 reporter for R7BP peptides (115/114 ratio is 0.192, $p=0.0008$; Fig. 3A). This likely reflects an ion suppression effects inherent to the application of iTRAQ® to complex mixtures[22]. In this scenario, other peptides within the ion selector mass tolerance window (5 Da) from the precursor peptide serve as source of the reporter ions while only precursor peptide is identified due to the ion suppression of others. These effects limit the application of this method for the quantification of proteins whose levels are down-regulated more than ~5 fold thus reaching the background threshold (116/114 ratio ~ 0.2). Since unequal amounts of RGS9-2 were precipitated from R7BP-/- and wild-type tissues, the data were normalized to bring 115:114 ratio of RGS9-2 protein to 1:1. The same correction factor was then applied to all proteins in the dataset using bias correction function built into the ProteinPilot™ software. Finally, in order to reliably account for the interactions that are not mediated by RGS9-2, but the level of which could non-specifically change between samples, we conducted additional immunoprecipitation experiments with RGS9-/- samples only. Proteins identified in these control experiments were excluded from the iTRAQ® dataset.

The final dataset revealed 21 binding partners of RGS9-2 that exhibit statistically significant upregulation upon elimination of R7BP (Table 1). The range of observed changes in levels varied from 2 to nearly 6 fold. Most of the identified proteins can be grouped into four distinct classes based on their roles in cellular processes. The largest class is represented by ribosomal proteins followed by equally represented cytoskeletal components, protein kinases and molecular chaperones. In summary, we have developed a quantitative proteomics method for analyzing interactome changes induced by genetic manipulation of mice and applied it to identify a distinct set of protein-protein interactions of RGS9/Gβ5 complex unregulated in response to the loss of its binding partner, R7BP.

Hsc70 is a new binding partner of RGS9-2 upregulated upon R7BP elimination

We have reasoned that decreased stability of RGS9-2 observed upon elimination of R7BP could be caused by the enhanced association of the complex with factors that mediate degradation of the RGS9-2/Gβ5 complex. This brought our attention to chaperone Hsc70, also

known as heat shock protein 8, a molecule that has been extensively implicated in protein degradation (reviewed in [23, 24]). Hsc70 shows ~5 fold upregulation in R7BP-/- samples and it is confidently identified by tandem mass-spectrometry screen with 7 peptides (15.2% sequence coverage) and 99% protein identification confidence as determined by ProteinPilot™ (see Fig. 4A for the representative MS/MS spectrum).

Western blot analysis revealed the presence of similar amounts of Hsc70 in the eluates from the immunoprecipitation experiments conducted with wild-type and R7BP-/- samples (Fig. 4B). Because substantially less RGS9-2 is precipitated from R7BP-/- samples as compared to wild type, this result indicates an increase in co-immunoprecipitation of Hsc70 with RGS9-2 in the absence of R7BP. Indeed, quantification of several Western blotting experiments revealed no statistically significant differences in Hsc70 levels between wild-type and R7BP-/- samples (ratio of band densities is 1.3±0.6, p=0.447). Therefore, when normalized to the 3.5-fold difference in RGS9-2 levels, these data indicate that the amount of Hsc-70 co-immunoprecipitated with RGS9-2 is increased by at least 3-fold, which is in good agreement with 5-fold Hsc70 upregulation quantified based on the iTRAQ® data.

The specificity of the Hsc70/RGS9-2 interaction in native neurons was validated by conducting the RGS9-2 immunoprecipitation experiments with striatal extracts obtained from RGS9-/- mice. The results presented in Fig. 4C show that while easily detectable in the wild-type eluates, Hsc70 is absent from the RGS9-/- samples confirming that the anti-RGS9-2 antibodies do not precipitate Hsc70 non-specifically. We further tested the interaction in transfected mammalian HEK293FT cells (Fig. 4D). As in native striatal neurons, RGS9-2/Gβ5 complex co-precipitated with Hsc70 endogenously expressed in HEK293 cells suggesting a direct nature of the binding that does not require the presence of specific neuronal proteins.

Hsc70 is recruited to the intrinsically disordered C-terminus of RGS9-2

We next addressed which molecular determinants in RGS9-2 mediate interaction with Hsc70. Previous studies have hypothesized that the loss of R7BP exposes KFERQ sequences confined to the N-terminal DEP/DHEX domains of RGS9-2 [9]. KFERQ motifs are known elements that confer Hsc70 recruitment [25]. Alternatively, Hsc70/Hsp70 chaperones have been shown to bind to the regions of high conformational flexibility known as intrinsic disorder regions [26, 27]. Analysis of RGS9-2 sequence by PONDR VSL2 algorithm [18, 19] of residue-by-residue prediction of the intrinsic disorder probability indicated that a proline-rich C-terminus is very likely to be intrinsically disordered (Fig. 5A). Most of the amino acid sequence of the C-terminal domain scores near a maximal probability value (PONDR VSL2 score 1), well above the score of the rest of the domains which are close to the threshold value of 0.5. These observations are additionally supported by the previously observed structure/functional similarity of RGS9-2 C-terminus to the gamma subunit of phosphodiesterase (PDE6γ) [15], a known intrinsically disordered protein [28, 29]. Therefore we have analyzed the interaction of Hsc70 with both of its potential binding sites in RGS9-2, the N-terminal fragment consisting of DEP and DHEX domains and C-terminal region (Fig. 5B). In transfected cells, the C-terminal domain of RGS9-2 co-precipitated with endogenous Hsc70. In contrast, immunoprecipitation of the N-terminal fragment did not reveal Hsc70 in the eluates above the amount that bound non-specifically to the beads, suggesting that its binding to Hsc70, if any, is much weaker than that of the C-terminus (Fig. 5B, right panels). Interestingly, binding of Hsc70 to RGS9-2 fragments inversely correlated with their expression levels in the cells (Fig. 5B left panels), consistent with the role of Hsc70 in mediating protein degradation.

Further proof that the C-terminus of RGS9-2 recruits Hsc70 was obtained from unbiased pull-down assays in which the His-tagged recombinant C-terminal fragment purified from Sf9 cells was covalently cross-linked to beads and incubated with total brain extract. Separation of the eluates by SDS PAGE followed by Coomasie staining revealed the presence of a single major

band retained by the protein-conjugated beads that was absent in the control experiment with empty beads (Fig. 5C). Tandem MS/MS mass-spectrometric analysis identified that this band contains a mixture of two chaperone proteins: Hsc70 (12 unique peptides) and its inducible homologue Hsp70 (9 unique peptides).

In the next set of experiments we have confirmed the specificity of the Hsc70 interaction with the C-terminus of RGS9-2 by performing forward and reciprocal co-immunoprecipitation experiments (Fig. 5D,E). Upon co-transfection in HEK293FT cells, c-myc-tagged Hsc70 construct was effectively co-precipitated with HA-tagged C-terminus of RGS9-2 when either c-myc or HA antibodies used for the immunoprecipitation but not in the control experiments in which cells were transfected only with one construct. Taking these data together, we conclude that intrinsically disordered C-terminus of RGS9-2 is a specific site mediating its binding to Hsc70.

Hsc70 regulates RGS9-2 expression

Our observation that Hsc70 specifically binds to destabilized RGS9-2 together with a known role of Hsc70 in protein degradation has prompted us to evaluate whether Hsc70 has an effect on RGS9-2 expression levels. We have first asked whether stabilization of RGS9-2/Gβ5 complex by R7BP affects its association with Hsc70. Consistent with earlier report [8], higher levels of RGS9-2 were detected in cells co-transfected with R7BP (Fig. 6A). Concomitantly, the presence of R7BP significantly reduced the amount of Hsc70 co-precipitating with RGS9-2/Gβ5 indicating that protective effects of R7BP involve down-regulation of Hsc70 binding to the complex (Fig. 6A,B).

We have next used an RNA interference approach to specifically knock-down Hsc70 and examine its effects on RGS9-2 levels. Transfection of cells with siRNA matching Hsc70 mRNA sequence resulted in 20.5±11.6% decrease in Hsc70 expression levels (Fig. 6C,D) as compared to control siRNA transfection ($p=0.015$, $n=6$, t-test). The modest degree of knockdown efficiency of Hsc70 is expected based on a critical housekeeping role that this protein plays for cellular survival [30]. Concomitant with Hsc70 down-regulation the levels of RGS9-2 increased by 17.4±6.1% ($p=0.002$, $n=6$, t-test) as evidenced by statistical analysis of quantitative Western blotting (Fig. 6D).

Further, we have employed a “dominant-negative” strategy aimed at inhibiting RGS9-2 interaction with Hsc70. The cells were additionally transfected with an excess of the construct encoding C-terminal domain of RGS9-2 which constitutes the main binding site for Hsc70 and therefore expected to compete with full-length RGS9-2 for binding to endogenous Hsc70. Data in Figure 6 (panels E and F) show that the expression of C-terminus in 2.5±0.3 -fold excess over full-length RGS9-2 (quantified by Western blotting) resulted in 2.0±0.3 -fold ($p=0.016$, $n=4$, t-test) increase in RGS9-2 expression. These data indicate that Hsc70 negatively regulates RGS9-2 expression consistent with their increased association upon RGS9-2 destabilization *in vivo*.

DISCUSSION

Proteomics approach for the analysis of changes in protein interaction networks in mouse genetic models

Many cellular functions are built on the principle of complex networks of protein-protein interactions. Recent studies in simple model organisms have indicated that most signaling proteins interact transiently and/or simultaneously with several partners [31]. While some interactions are static, growing evidence suggests that the majority of proteins are part of macromolecular assemblies where individual components transiently interact with each other

[31, 32]. Thus, it is the dynamic re-organization of these networks that is thought to be responsible for mediating a variety of cellular reactions including signal transmission, biogenesis and trafficking of molecules, and formation of cellular structures [33, 34].

The interaction dynamics of signaling proteins in mammals is relatively uncharted territory. It is generally recognized that the logic behind addressing such questions in a complex signaling networks, such as those in neurons for example, is to study perturbations in the cellular interactome that occur following specific protein changes (see [35] for discussion). An increasing number of studies have reported changes in protein expression following specific manipulations (see [36, 37] for recent examples) as well as comprehensive information about the intearactome for individual proteins [38, 39]. However, the analysis of the changes in the interaction profiles following precise intervention at the level of a single molecule is substantially lagging, although such studies are expected to provide valuable insights into the operational logic of the signaling pathways and the mechanisms of their regulation.

Genetic mouse models represent potentially powerful tools for examining the interactome changes in mammalian systems. A variety of mouse knockout and transgenic strains offer precise control over the expression of a single gene often with an exquisite spatial and temporal resolution making them uniquely suited delineating dynamic interactions in complex signaling networks but also for performing interaction specificity controls critical for validitation of interactome data. In this study, we report the development of a proteomics approach to quantify changes in the protein interactions induced by genetic knockout, and demonstrate its application for studying the mechanisms mediating the degradation of RGS9-2, a key regulator of G protein signaling in the striatum. The platform for this approach is antibody-based affinity purification of protein complexes followed by differential iTRAQ® labeling of samples, and subsequent mass-spectrometric identification and quantification of binding proteins. The use of two separate types of mouse knockouts is critical for the success of the approach. The first line lacks the component whose influence on the interaction network is being studied. The second line lacks the target protein for the affinity purification, and therefore provides the ideal control for interaction specificity. Following mass-spectrometric quantification and normalization to the levels of purified proteins, the resulting interactome database is expected to reveal three groups of proteins whose interaction within the complex are: (i) up-regulated, (ii) down-regulated, or (iii) unchanged. Grouping these proteins by homology or functional relevance provides insight into how changes in the interactions of the central protein of interest translate into regulation of its functional homeostasis and/or changes in signaling networks. In our application of the approach, we have focused on identifying interactions that are upregulated upon decrease in the levels of signaling protein undergoing degradation. Due to the large decrease in target protein levels, the identification of the interactome alterations was limited to up-regulated of interactions, as down-regulated associations fell close to the threshold for identification set by the non-specificity control provided by the knockout of the target protein and therefore could not be considered reliable. Nevertheless, we believe this approach may be successfully used for the identification of changes in the interactome in both directions providing that the levels of the target proteins do not exhibit substantial differences. Given the nature of the alteration in the knockout mouse of interest, the results reported in the present study primarily describe the identification of the mechanisms for regulation of signaling protein homeostasis. However, we envision that future applications of the described approach to other signaling systems could also result in the identification of a range of functional interaction changes.

Insights into mechanisms of RGS9-2 degradation from interactome analysis

The abundance of RGS9-2 in the striatum has been demonstrated to influence sensitivity of reward and motor circuits in D2-dopamine and μ-opioid receptor signaling pathways [13, 40,

[41]. Interestingly, stimulation of the receptors by psychostimulants and morphine [11, 13, 40, 41], changes in neuronal excitability and oxygenation status[10] have been shown to result in rapid changes in RGS9-2 expression, which is thought to constitute an important feedback mechanism underlying the plasticity of striatal signaling [3]. Dynamic association with the membrane anchor R7BP has been shown to play a key role in controlling the expression of RGS9-2 by altering proteolytic stability of the complex [9, 10]. The key observation of this study is the identification of a molecular chaperone Hsc70 that is a critical factor negatively regulating RGS9-2 expression levels that are upregulated upon the loss of R7BP binding. How can Hsc70 association lead to the degradation of RGS9-2? Hsc70 is a major housekeeping isoform of the Hsp70 family of chaperone proteins[42, 43]. Abundant evidence indicates that, in addition to protein folding, Hsc70 plays a major role in protein degradation. There are two distinct mechanisms by which Hsc70 is known to assist in protein degradation. On the one hand, Hsc70 recruits the E3 ubiquitin ligase CHIP to its substrate protein facilitating ubiquitination and subsequent proteasomal degradation[24, 44]. On the other hand, Hsc70 in complex with co-chaperone proteins binds to the LAMP2a channel and targets proteins for import into the lysosomes where they undergo degradation through a process called chaperone-mediated autophagy [23, 45]. Proteolysis of RGS9-2 in the striatum of R7BP mice can be prevented by blocking cysteine proteases but not the proteasome suggesting that the lysosomal pathway is likely to be responsible for the degradation of RGS9-2 [9]. However, in transfected cells, RGS9-2 was also found to be ubiquitinated in R7BP-sensitive manner[10]. These observations suggest that the mechanism of RGS9-2 degradation might be complex and involve post-translational modifications, i.e. ubiquitination, in addition to Hsc70-based chaperone mediated autophagy. For example, three protein kinases found on the list of the up-regulated interactions could also be involved in specifying the pathway of RGS9-2 degradation *in vivo*. In any event, we believe that the involvement of Hsc70 in both pathways makes it a key regulator of RGS9-2 expression.

We have shown that the main site of Hsc70 binding is located within the intrinsically disordered C-terminus of RGS9-2. This observation is consistent with a previous report that Hsc70 is recruited to an intrinsically disordered domain of the TNF-α regulator SIMPL [27] and further implicates Hsc70 as a sensor of the intrinsic disorder regions in proteins. Previously, the only universal consensus site in proteins for Hsc70 binding was thought to be formed by so-called 'KFERQ' sequences. These motifs have poor conservation and high variability between different proteins, the hallmark feature of which is a hydrophobic, highly positive and highly negative stretch of 5-6 amino acids [45]. Interestingly, the N-terminus of RGS9-2 was predicted to contain several KFERQ-like motifs located within the local intrinsic disorder peaks. Several KFERQ-like sequences were also predicted within the C-terminal domain, which incidentally exhibits much longer regions of disorder. Because C-terminal domain of RGS9-2 binds Hsc70 much stronger than the N-terminal region we conclude that a combination of high intrinsic disorder propensity with the presence of the "KFERQ"-like motif is a stronger predictor of Hsc70 recruitment than the presence of the 'KEFRQ'-like sequences alone. In fact, our analysis of intrinsic disorder indicates that 'KFERQ'-like sequences are extremely likely to be unstructured suggesting that these sequences represent local disorder hot-spots. Therefore, the intrinsic disorder domains in proteins are likely to serve as the primary determinant for the interaction of target proteins with Hsc70 chaperons, thus determining their rate of turnover in the cell.

Beyond Hsc70, ribosomal proteins were a major group of RGS9-2 binding proteins that were upregulated in R7BP knockout tissue. The crystal structure of the ribosome [46] indicates that most of the ribosomal proteins we isolated are clustered on the surface of the ribosomal subunits suggesting that they likely reflect the interaction of the nascent RGS9-2 chain with ribosomes. In fact, ribosomal proteins often serve as the initial interaction partners for newly synthesized proteins, thus assisting in their folding (see [47] for recent review). This suggests a co-translational mechanism of RGS9-2 complex assembly with R7BP. Furthermore, chaperones

of the Hsp70 family, including Hsc70 are found bound to the ribosomes where they are thought to facilitate folding and macromolecular complex assembly [48, 49]. This leads us to hypothesize a scenario for co-translational checkpoint control of the formation of the RGS9-2/R7BP complex. We speculate that newly emerging DEP/DHEX domains of RGS9-2 bind to R7BP causing this complex to be quickly targeted to its destination in the post-synaptic density. In the absence of R7BP, lingering transient interactions with ribosomal proteins lead to the recruitment of ribosome associated Hsc70 to the C-terminus of RGS9-2 resulting in degradation. Finally, increased association of RGS9-2 with cytoskeletal proteins in the absence of R7BP could be explained by the fact that both ribosomes and Hsp70 chaperones are organized by the cytoskeleton [50, 51]. In conclusion, we believe that precise delineation of the pathways and regulatory cues that are responsible for triggering RGS9-2 proteolysis will be an exciting future direction, and we hope further investigation of the regulated RGS9-2 binding partners our study has uncovered will provide insight into this process.

SYNOPSIS

Quantitative *in vivo* interactome analysis conducted with strains of genetically modified mice identified molecular chaperone Hsc70 as a regulator of RGS9-2/Gb5 expression levels.

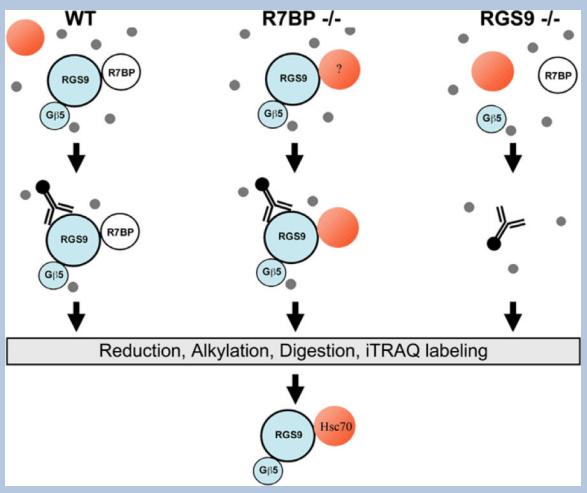

Acknowledgments

We are indebted to Dr. LeeAnn Higgins at the Center for Mass-Spectrometry and Proteomics, University of Minnesota for the acquisition of the mass-spectrometry data, discussions and critical comments on the manuscript. We are grateful to Drs. Brock Grill, Nick Skiba and Garret Anderson for critical comments on the manuscript. We also thank Dr. William Simonds (NIH) for the generous gift of anti-R7BP and anti-Gβ5 antibodies, Dr. Jason Chen (Virginia Commonwealth University) for providing RGS9 knockout mice, Dr. Cam Patterson for providing Hsc70 construct, Dr. Keqiang Xie for cloning HA-tagged N-terminus of RGS9-2. This work was supported in part by NIH grants DA021743 (K.A.M.), DA026405 (K.A.M.), LM007688 (V.N.U.) and GM071714 (V.N.U.), McKnight Land-Grant Professorship award (K.A.M.), and a grant from the Program of the Russian Academy of Sciences “Molecular and Cellular Biology” (V.N.U.). We gratefully acknowledge core resources [rovided by Minnesota Supercomputing Institute and the support of the IUPUI Signature Centers Initiative. National Science Foundation for Major Research Instrumentation grants 9871237 and NSF-DBI-0215759 was used to purchase the instruments described in this study

REFERENCES

1. Anderson GR, Posokhova E, Martemyanov KA. The R7 RGS protein family: multi-subunit regulators of neuronal G protein signaling. Cell Biochem Biophys 2009;54:33–46. [PubMed: 19521673]

2. Martemyanov, KA.; Arshavsky, VY. Biology and functional regulation of RGS9 isoforms. In: Fisher, R., editor. Progress in Molecular Biology and Translational Science. Academic Press; 2009. p. 205-227.
3. Traynor JR, Terzi D, Caldarone BJ, Zachariou V. RGS9-2: probing an intracellular modulator of behavior as a drug target. Trends Pharmacol Sci 2009;30:105–11. [PubMed: 19211160]
4. Kovoor A, Chen CK, He W, Wensel TG, Simon MI, Lester HA. Co-expression of Gbeta5 enhances the function of two Ggamma subunit-like domain-containing regulators of G protein signaling proteins. J Biol Chem 2000;275:3397–402. [PubMed: 10652332]
5. Martemyanov KA, Yoo PJ, Skiba NP, Arshavsky VY. R7BP, a novel neuronal protein interacting with RGS proteins of the R7 family. J Biol Chem 2005;280:5133–6. [PubMed: 15632198]
6. Chen CK, Eversole-Cire P, Zhang H, Mancino V, Chen YJ, He W, Wensel TG, Simon MI. Instability of GGL domain-containing RGS proteins in mice lacking the G protein beta-subunit Gbeta5. Proc Natl Acad Sci U S A 2003;100:6604–9. [PubMed: 12738888]
7. Drenan RM, Doupnik CA, Boyle MP, Muglia LJ, Huettner JE, Linder ME, Blumer KJ. Palmitoylation regulates plasma membrane-nuclear shuttling of R7BP, a novel membrane anchor for the RGS7 family. J Cell Biol 2005;169:623–33. [PubMed: 15897264]
8. Anderson GR, Semenov A, Song JH, Martemyanov KA. The membrane anchor R7BP controls the proteolytic stability of the striatal specific RGS protein, RGS9-2. J Biol Chem 2007;282:4772–81. [PubMed: 17158100]
9. Anderson GR, Lujan R, Semenov A, Pravetoni M, Posokhova EN, Song JH, Uversky V, Chen CK, Wickman K, Martemyanov KA. Expression and localization of RGS9-2/G 5/R7BP complex in vivo is set by dynamic control of its constitutive degradation by cellular cysteine proteases. J Neurosci 2007;27:14117–27. [PubMed: 18094251]
10. Anderson GR, Lujan R, Martemyanov KA. Changes in striatal signaling induce remodeling of RGS complexes containing Gbeta5 and R7BP subunits. Mol Cell Biol 2009;29:3033–44. [PubMed: 19332565]
11. Burchett SA, Bannon MJ, Granneman JG. RGS mRNA expression in rat striatum: modulation by dopamine receptors and effects of repeated amphetamine administration. J Neurochem 1999;72:1529–33. [PubMed: 10098858]
12. Zachariou V, Georgescu D, Sanchez N, Rahman Z, DiLeone R, Berton O, Neve RL, Sim-Selley LJ, Selley DE, Gold SJ, Nestler EJ. Essential role for RGS9 in opiate action. Proc Natl Acad Sci U S A 2003;100:13656–61. [PubMed: 14595021]
13. Rahman Z, Schwarz J, Gold SJ, Zachariou V, Wein MN, Choi KH, Kovoor A, Chen CK, DiLeone RJ, Schwarz SC, Selley DE, Sim-Selley LJ, Barrot M, Luedtke RR, Self D, Neve RL, Lester HA, Simon MI, Nestler EJ. RGS9 modulates dopamine signaling in the basal ganglia. Neuron 2003;38:941–52. [PubMed: 12818179]
14. Skiba NP, Martemyanov KA, Elfenbein A, Hopp JA, Bohm A, Simonds WF, Arshavsky VY. RGS9-Gbeta5 substrate selectivity in photoreceptors - Opposing effects of constituent domains yield high affinity of RGS interaction with the G protein-effector complex. J Biol Chem 2001;276:37365–37372. [PubMed: 11495924]
15. Martemyanov KA, Hopp JA, Arshavsky VY. Specificity of G protein-RGS protein recognition is regulated by affinity adapters. Neuron 2003;38:857–862. [PubMed: 12818172]
16. Chen CK, Burns ME, He W, Wensel TG, Baylor DA, Simon MI. Slowed recovery of rod photoresponse in mice lacking the GTPase accelerating protein RGS9-1. Nature 2000;403:557–560. [PubMed: 10676965]
17. Shevchenko A, Tomas H, Havlis J, Olsen JV, Mann M. In-gel digestion for mass spectrometric characterization of proteins and proteomes. Nat Protoc 2006;1:2856–60. [PubMed: 17406544]
18. Obradovic Z, Peng K, Vucetic S, Radivojac P, Dunker AK. Exploiting heterogeneous sequence properties improves prediction of protein disorder. Proteins 2005;7(61 Suppl):176–82. [PubMed: 16187360]
19. Peng K, Vucetic S, Radivojac P, Brown CJ, Dunker AK, Obradovic Z. Optimizing long intrinsic disorder predictors with protein evolutionary information. J Bioinform Comput Biol 2005;3:35–60. [PubMed: 15751111]

20. Zieske LR. A perspective on the use of iTRAQ reagent technology for protein complex and profiling studies. J Exp Bot 2006;57:1501–8. [PubMed: 16574745]
21. Shilov IV, Seymour SL, Patel AA, Loboda A, Tang WH, Keating SP, Hunter CL, Nuwaysir LM, Schaeffer DA. The Paragon Algorithm, a next generation search engine that uses sequence temperature values and feature probabilities to identify peptides from tandem mass spectra. Mol Cell Proteomics 2007;6:1638–55. [PubMed: 17533153]
22. Ow SY, Salim M, Noirel J, Evans C, Rehman I, Wright PC. iTRAQ underestimation in simple and complex mixtures: “the good, the bad and the ugly”. J Proteome Res 2009;8:5347–55. [PubMed: 19754192]
23. Dice JF. Chaperone-mediated autophagy. Autophagy 2007;3:295–9. [PubMed: 17404494]
24. McDonough H, Patterson C. CHIP: a link between the chaperone and proteasome systems. Cell Stress Chaperones 2003;8:303–8. [PubMed: 15115282]
25. Massey AC, Zhang C, Cuervo AM. Chaperone-mediated autophagy in aging and disease. Curr Top Dev Biol 2006;73:205–35. [PubMed: 16782460]
26. Radivojac P, Iakoucheva LM, Oldfield CJ, Obradovic Z, Uversky VN, Dunker AK. Intrinsic disorder and functional proteomics. Biophys J 2007;92:1439–56. [PubMed: 17158572]
27. Haag Breese E, Uversky VN, Georgiadis MM, Harrington MA. The disordered amino-terminus of SIMPL interacts with members of the 70-kDa heat-shock protein family. DNA Cell Biol 2006;25:704–14. [PubMed: 17233114]
28. Song J, Guo LW, Muradov H, Artemyev NO, Ruoho AE, Markley JL. Intrinsically disordered gamma-subunit of cGMP phosphodiesterase encodes functionally relevant transient secondary and tertiary structure. Proc Natl Acad Sci U S A 2008;105:1505–10. [PubMed: 18230733]
29. Uversky VN, Permyakov SE, Zagranichny VE, Rodionov IL, Fink AL, Cherskaya AM, Wasserman LA, Permyakov EA. Effect of zinc and temperature on the conformation of the gamma subunit of retinal phosphodiesterase: a natively unfolded protein. J Proteome Res 2002;1:149–59. [PubMed: 12643535]
30. Rohde M, Daugaard M, Jensen MH, Helin K, Nylandsted J, Jaattela M. Members of the heat-shock protein 70 family promote cancer cell growth by distinct mechanisms. Genes Dev 2005;19:570–82. [PubMed: 15741319]
31. Jeong H, Mason SP, Barabasi AL, Oltvai ZN. Lethality and centrality in protein networks. Nature 2001;411:41–2. [PubMed: 11333967]
32. Han JD, Bertin N, Hao T, Goldberg DS, Berriz GF, Zhang LV, Dupuy D, Walhout AJ, Cusick ME, Roth FP, Vidal M. Evidence for dynamically organized modularity in the yeast protein-protein interaction network. Nature 2004;430:88–93. [PubMed: 15190252]
33. Cusick ME, Klitgord N, Vidal M, Hill DE. Interactome: gateway into systems biology. Hum Mol Genet 2005;14:R171–81. Spec No. 2. [PubMed: 16162640]
34. Devos D, Russell RB. A more complete, complexed and structured interactome. Curr Opin Struct Biol 2007;17:370–7. [PubMed: 17574831]
35. Wilkins MR, Kummerfeld SK. Sticking together? Falling apart? Exploring the dynamics of the interactome. Trends Biochem Sci 2008;33:195–200. [PubMed: 18424047]
36. Liu L, Channavajhala PL, Rao VR, Moutsatsos I, Wu L, Zhang Y, Lin LL, Qiu Y. Proteomic characterization of the dynamic KSR-2 interactome, a signaling scaffold complex in MAPK pathway. Biochim Biophys Acta 2009;1794:1485–95. [PubMed: 19563921]
37. Iff J, Wang W, Sajic T, Oudry N, Gueneau E, Hopfgartner G, Varesio E, Szanto I. Differential Proteomic Analysis of STAT6 Knockout Mice Reveals New Regulatory Function in Liver Lipid Homeostasis. J Proteome Res. 2009
38. Paulo J, Brucker W, Hawrot E. Proteomic Analysis of an 7 Nicotinic Acetylcholine Receptor Interactome. J Proteome Res. 2009
39. Bai Y, Markham K, Chen F, Weerasekera R, Watts J, Horne P, Wakutani Y, Bagshaw R, Mathews PM, Fraser PE, Westaway D, St George-Hyslop P, Schmitt-Ulms G. The in vivo brain interactome of the amyloid precursor protein. Mol Cell Proteomics 2008;7:15–34. [PubMed: 17934213]
40. Psifogeorgou K, Papakosta P, Russo SJ, Neve RL, Kardassis D, Gold SJ, Zachariou V. RGS9-2 is a negative modulator of mu-opioid receptor function. J Neurochem 2007;103:617–25. [PubMed: 17725581]

41. Zachariou V, Georgescu D, Sanchez N, Rahman Z, DiLeone R, Berton O, Neve RL, Sim-Selley LJ, Selley DE, Gold SJ, Nestler EJ. Essential role for RGS9 in opiate action. Proc Natl Acad Sci USA 2003;100:13656–13661. [PubMed: 14595021]

42. Lindquist S, Craig EA. The heat-shock proteins. Annu Rev Genet 1988;22:631–77. [PubMed: 2853609]

43. Daugaard M, Rohde M, Jaattela M. The heat shock protein 70 family: Highly homologous proteins with overlapping and distinct functions. FEBS Lett 2007;581:3702–10. [PubMed: 17544402]

44. Qian SB, Princiotta MF, Bennink JR, Yewdell JW. Characterization of rapidly degraded polypeptides in mammalian cells reveals a novel layer of nascent protein quality control. J Biol Chem 2006;281:392–400. [PubMed: 16263705]

45. Majeski AE, Dice JF. Mechanisms of chaperone-mediated autophagy. Int J Biochem Cell Biol 2004;36:2435–44. [PubMed: 15325583]

46. Yusupov MM, Yusupova GZ, Baucom A, Lieberman K, Earnest TN, Cate JH, Noller HF. Crystal structure of the ribosome at 5.5 A resolution. Science 2001;292:883–96. [PubMed: 11283358]

47. Kramer G, Boehringer D, Ban N, Bukau B. The ribosome as a platform for co-translational processing, folding and targeting of newly synthesized proteins. Nat Struct Mol Biol 2009;16:589–97. [PubMed: 19491936]

48. Frydman J. Folding of newly translated proteins in vivo: the role of molecular chaperones. Annu Rev Biochem 2001;70:603–47. [PubMed: 11395418]

49. Bukau B. Ribosomes catch Hsp70s. Nat Struct Mol Biol 2005;12:472–3. [PubMed: 15933729]

50. Liang P, MacRae TH. Molecular chaperones and the cytoskeleton. J Cell Sci 1997;110(Pt 13):1431–40. [PubMed: 9224761]

51. Hovland R, Hesketh JE, Pryme IF. The compartmentalization of protein synthesis: importance of cytoskeleton and role in mRNA targeting. Int J Biochem Cell Biol 1996;28:1089–105. [PubMed: 8930133]

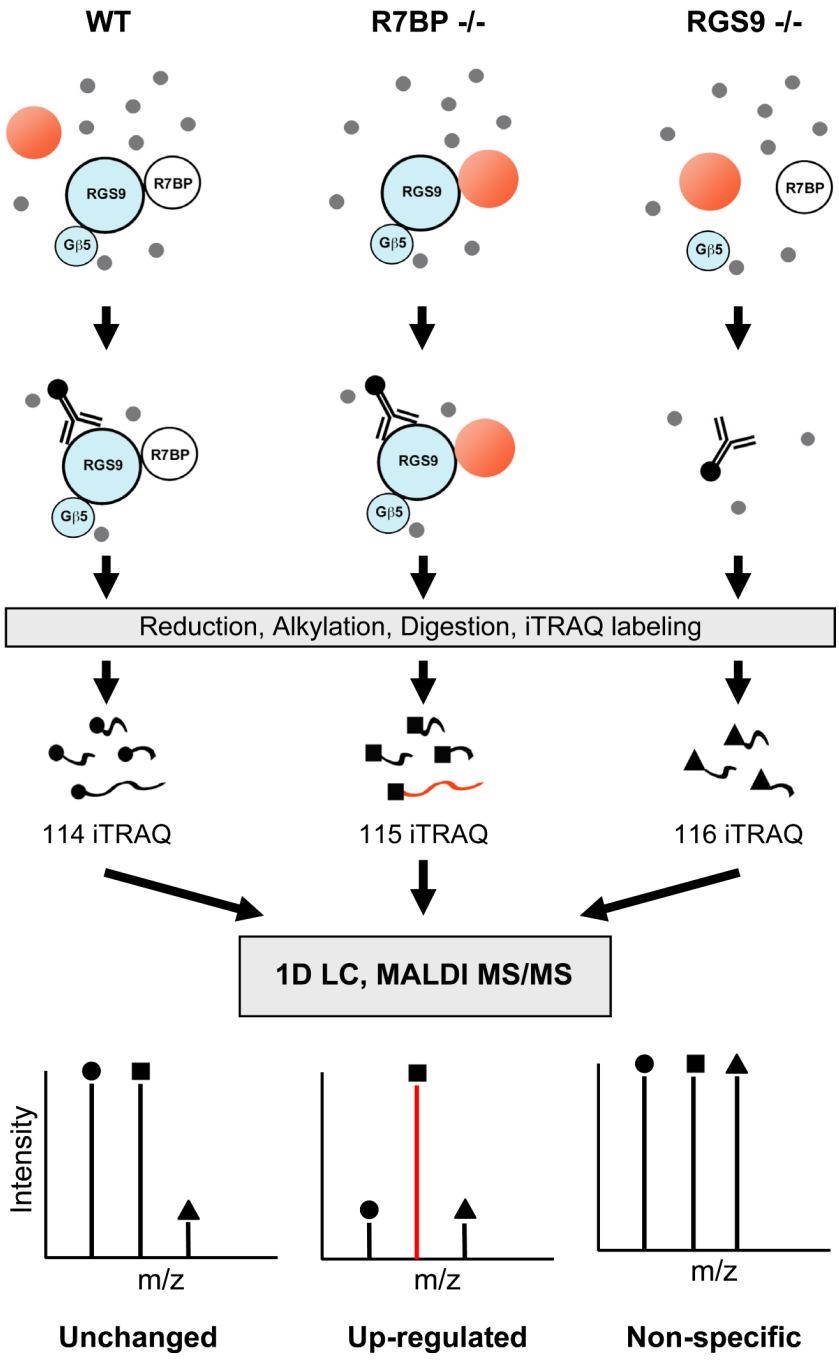

Figure 1. Approach for quantitative and comparative analysis of changes in the RGS9-2 interactome in genetic mouse models

Striatal lysates were prepared from wild-type (WT), R7BP knockout (R7BP-/-), or RGS9 knockout (RGS9-/-) animals. RGS9-2 containing complexes were purified in parallel with specific antibodies that recognize the C-terminus of RGS9-2, and eluates were reduced, alkylated and digested with trypsin. Peptides were differentially labeled with iTRAQ® labels, as indicated, i.e. iTRAQ®114 label (•) was used for WT, iTRAQ®115 (■) - for R7BP-/-, and iTRAQ®116. (▲) - for RGS9-/- samples. Samples were combined and the mixture was resolved by one dimensional liquid chromatography (1D LC), mixed with matrix solution and continuously spotted on a MALDI target. Samples were analyzed by tandem mass spectrometry

using ABI 4800 MALDI TOF/TOF analyzer followed by protein identification and quantification using ProteinPilot software. It is theoretically expected that interactions that are up-regulated in R7BP-/- samples will show higher intensity of iTRAQ®115 ions. Non-specific interactions that are found in RGS9-/- samples and do not show differences in iTRAQ® label intensities are excluded from the analysis.

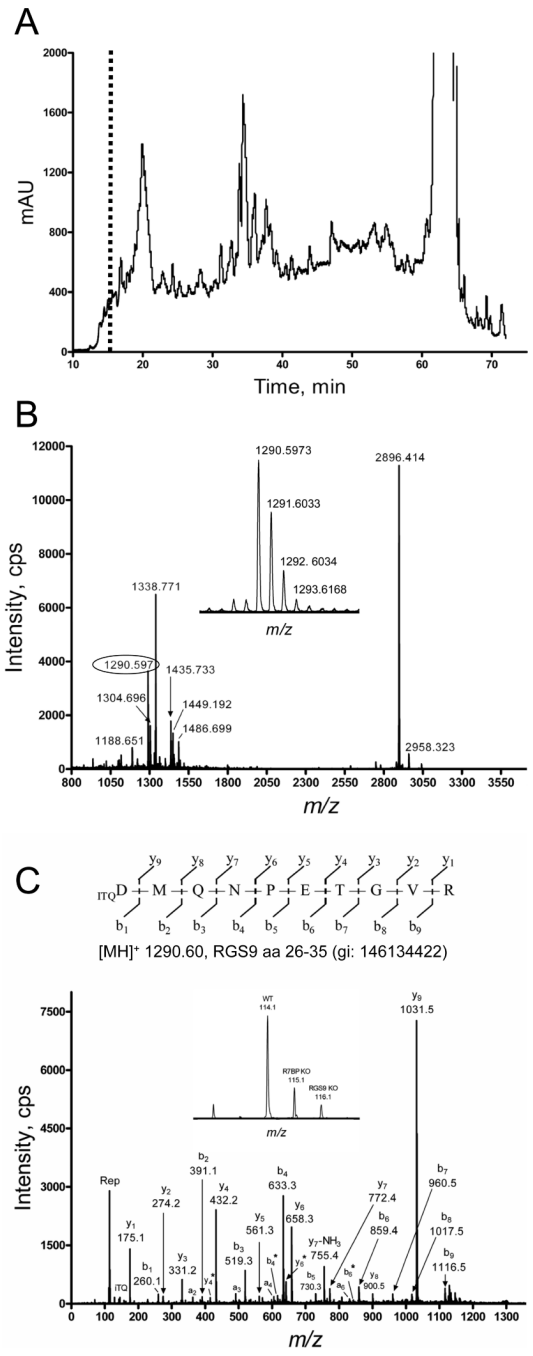

Figure 2. Identification and quantification of changes in RGS9-2 interaction partners

A, Separation profile of the peptide elution from analytical C18 as detected by absorbtion at λ=214. The dashed vertical line indicates a representative fraction subjected to MS analysis (*panel B*, below). **B**, A representative full scan MS spectrum of the fraction/spot eluted from analytical C18 column at the time point indicated in *panel A. Insert*: high resolution graph showing precursor region of the ion selected for tandem MS/MS shown in *panel C*. **C**, representative MS/MS fragmentation spectrum, generated by precursor ion at m/z 1290.60. Continuous series of both b- and y-ions allowed high confidence assignment of the amino acid sequence DMQNPETGVR, corresponding to aa 26-35 of RGS9-2 sequence. *Insert*: high resolution graph showing iTRAQ® reporter region. All graphs were exported as ASCII files

and peaks were labeled in GraphPad Prism. Abbreviations are: mAU, milliabsorbance units; aa, aminoacids; cps, counts per second; Rep, iTRAQ® reporter ions.

A

Name	% Cov (p-value)	Number of peptides	115:114 (p-value)	116:114 (p-value)
RGS9-2 (gi: 146134422)	**65.78** ($5.32x10^{-100}$)	**72**	**0.206** ($4.02x10^{-28}$)	**0.162** ($3.01x10^{-20}$)
Gβ5 (gi: 6754018, 41281679)	**40** ($8.63x10^{-29}$)	**22**	**0.313** ($5.04x10^{-7}$)	**0.350** (0.002)
R7BP (gi: 119360350)	**29.18** ($9.96x10^{-11}$)	**7**	**0.192** (0.0008)	**0.247** (0.015)

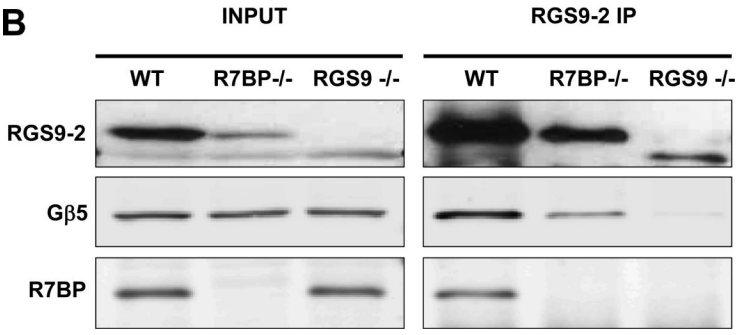

Figure 3. Quantification of the composition of the RGS9-2 core complex by iTRAQ® and Western blotting

A, Summary of identification and iTRAQ®-based quantification of known binding partners of RGS9-2 performed by ProteinPilot software. In cases where a set of peptides could be assigned to more than one protein, all accession numbers are listed. Percent coverage and number of peptides refer to the peptides with at least 95% identification confidence according to ProteinPilot. *p-values* for the identification and change significance are as reported by Protein Pilot software. **B**, Quantitative immunoblotting of RGS9-2 containing complexes immunoprecipitated from wild-type (WT), R7BP knockout (R7BP-/-), and RGS9 knockout (RGS9-/-) striatal tissues. Whole cell extracts (Input) and eluates from beads conjugated to RGS9-2 antibodies (RGS9 IP) were analyzed by quantitative Western blotting using secondary antibodies labeled with IRDye680 and IRDye800 fluorescent dyes and detected by an Odyssey (LiCor) infrared scanner. Immunoprecipitation and elution was performed as described in Materials and Methods. Equal protein amounts of striatal extracts and volumes of eluates were loaded on the gel.

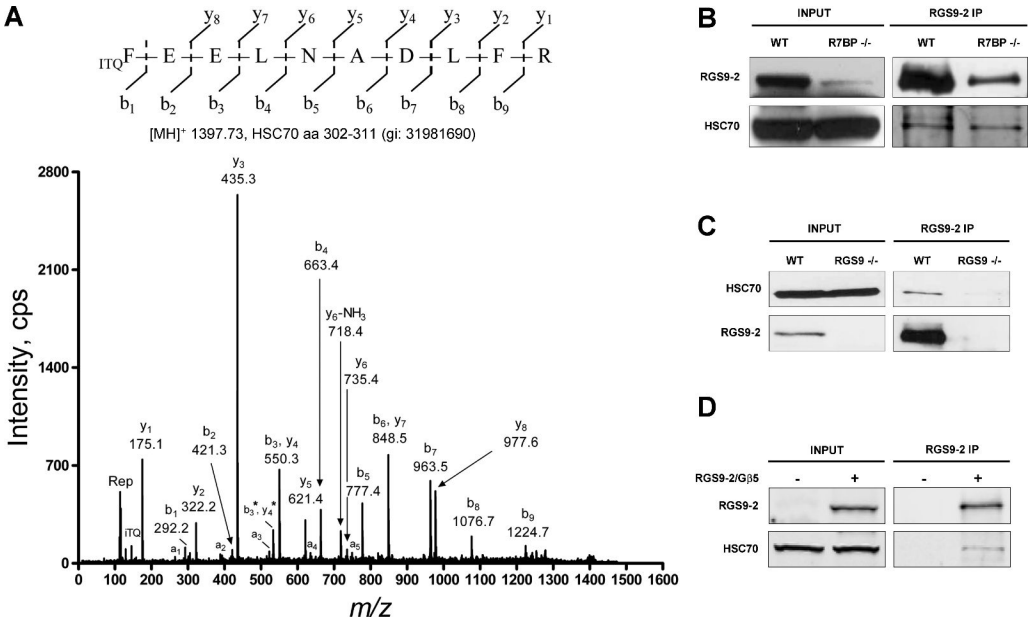

Figure 4. Hsc70 is a binding partner of RGS9-2

A, Representative MS/MS spectrum and deduced amino acid sequence of an Hsc70-derived peptide found in RGS9-2 immunoprecipitation. **B**, Co-immunoprecipitation of Hsc70 with RGS9-2 from wild-type and R7BP knockout striatal tissues. RGS9-2 was immunoprecipitated and eluates were subjected to Western blot analysis as described under *Experimental Procedures*. **C**, Hsc70 is absent from the eluates from RGS9-/- samples indicating specific interaction between RGS9-2 and Hsc70. RGS9-2 was precipitated with a specific antibody from striatal lysates of wild-type (WT) and RGS9 knockout (RGS9-/-) mice and analyzed by Western blotting. **D**, Hsc70 interacts with RGS9-2 in transfected cells. HEK293FT cells were co-transfected with equal amounts of either RGS9-2/Gβ5 complex or empty pcDNA3.1 vector. RGS9-2 was precipitated with a specific antibody and eluates were analyzed by Western blotting.

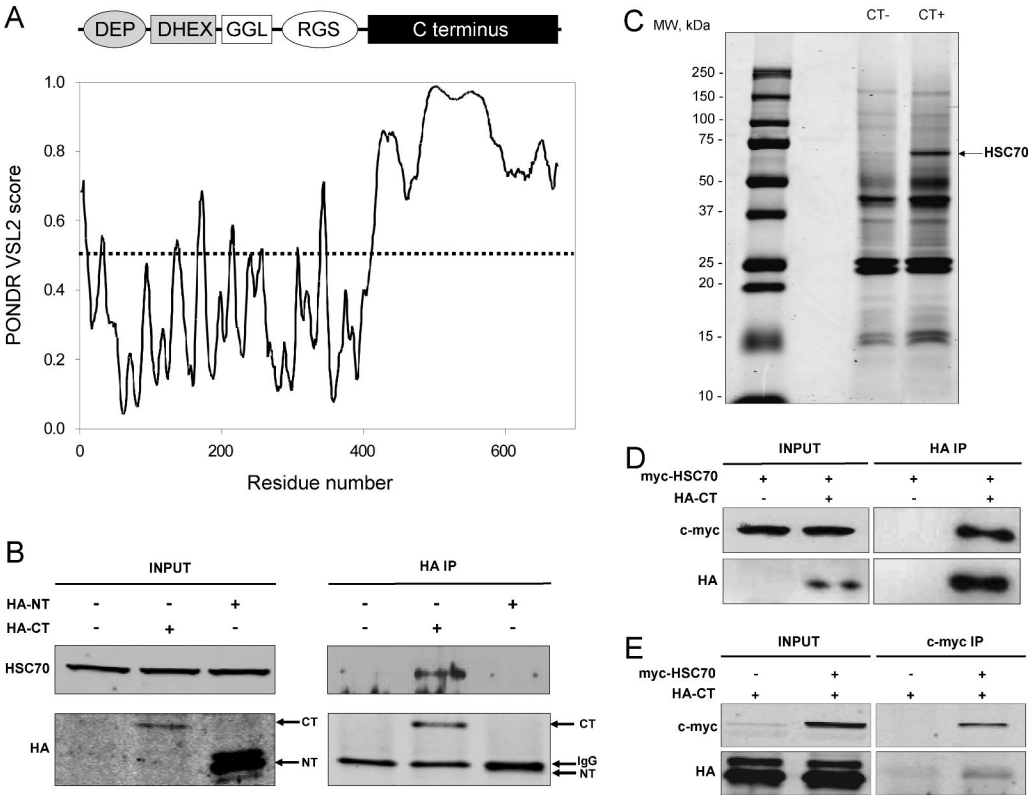

Figure 5. The interaction of Hsc70 with RGS9-2 is mediated by the C-terminus of RGS9-2

A, Intrinsic disorder prediction for RGS9-2 sequence using PONDR VSL2 algorithm. A dashed line represents an arbitrary threshold for disorder set at 0.5 value. Gray shading represents N-terminus and black marks the C-terminal fragments of RGS9-2 used in the subsequent experiments (panels B,C,D,E). **B**, Comparison of Hsc70 binding to N-terminal (NT) and C-terminal (CT) fragments of RGS9-2. HEK293 cells were transfected with either C-terminus or N-terminus. Both the C- and N-terminus were tagged with an HA tag, which was used for their precipitation from cellular lysates, followed by analysis with Western blotting. **C,** A Coomasie stained gel showing separation of proteins pulled-down from whole brain extracts by either empty SulphoLink beads (-CT) or SulphoLink beads conjugated to the recombinant C-terminus of RGS9-2 (+CT). Arrow indicates a position of the band specifically present in +CT but not -CT samples. MALDI MS/MS analysis identified Hsc70 as a major protein present in the band. **D**, Co-immunoprecipitation of HA-tagged C-terminus of RGS9-2 (HA-CT) with myc-tagged Hsc70 (myc-Hsc70) from transfected HEK293 cells using anti anti-HA antibody, followed by Western blotting analysis. **E**, Reciprocal co-immunoprecipitation of HA-tagged C-terminus of RGS9-2 with myc-tagged Hsc70 from transfected HEK293FT cells using anti c-myc antibody, followed by Western blotting analysis.

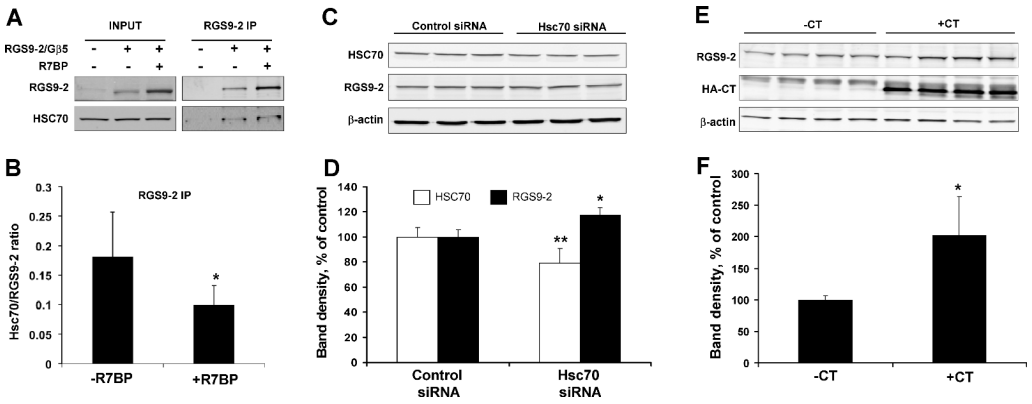

Figure 6. Hsc70 is a negative regulator of RGS9-2 expression

A, Down-regulation of Hsc70 binding to RGS9-2/Gβ5 upon co-expression with R7BP. HEK293 cells were transfected with RGS9-2/Gβ5 complex with either R7BP or empty pcDNA3.1 vector. RGS9-2 containing complexes were immunoprecipitated from cell lysates and eluates were analyzed using specific antibodies. **B,** Quantification of changes in Hsc70 binding analyzed as described in panel A. Band densities were quantified by Odyssey infrared imaging system and integrated intensities were normalized to the amounts of precipitated RGS9-2.

C, Up-regulation of RGS9-2 expression upon knock-down of Hsc70. HEK293FT cells were transfected with either negative control siRNA or specific siRNA targeting Hsc70 expression, followed by transfection with RGS9-2/Gβ5 complex. Twenty four hrs post transfection, cell lysates (20 μg/lane) were analyzed for protein expression using specific antibodies. **D**, Quantification of changes in expression levels of proteins analyzed as described in panel C. Band densities were quantified by Odyssey infrared imaging system and integrated intensities were normalized to β-actin. **E**, Up-regulation of RGS9-2 expression upon co-expression of the C-terminus of RGS9-2 (CT). HEK293FT cells were transfected with RGS9-2/Gβ5 complex (0.25 μg each/10 cm^2) with either C-terminus (+CT) or empty pcDNA 3.1 vector (-CT) (2 μg/10 cm^2). Twenty four hrs after transfection cell lysates (20 μg/lane) were analyzed for protein expression using RGS9-2 and β-actin antibodies. **F**, Quantification of changes in expression levels of proteins, presented in panel E. Band densities were quantified by Odyssey infrared imaging system and normalized to β-actin.

Asterisk indicates a statistically significant difference ($p<0.05$) as revealed by Student's t-test.

Table 1

Proteins showing up-regulated binding to RGS9-2 in R7BP-/- samples

Protein Name	Accession	Fold increase	Normalized 114/115 ratio	p-value of ratio	Number of peptides	%Coverage	ID score	p-value of ID
predicted hypothetical protein similar to Igh-1a	gi|149274201	5.6	0.179	2.5×10^{-4}	5	38.22	10.02	9.5×10^{-11}
p21 (CDKN1A)-activated kinase 7	gi|134949024	5.4	0.184	3.9×10^{-8}	7	21.56	17.34	4.5×10^{-18}
heat shock protein 8 (Hsc70)	gi|31981690	5.2	0.192	5.6×10^{-8}	7	18.27	14	9.9×10^{-15}
2′,3′-cyclic nucleotide 3′ phosphodiesterase	gi|6753476	5.2	0.193	0.0201	2	9.05	4	1.0×10^{-4}
ribosomal protein L13	gi|33186863	5	0.202	1.5×10^{-4}	4	23.70	8.09	8.1×10^{-9}
calcium/calmodulin-dependent protein kinase II α2	gi|28916677	4.9	0.204	0.0123	1	3.14	2.31	0.0049
predicted hypothetical protein similar to IgG	gi|149255583	4.5	0.224	0.006	3	29.75	6	1.0×10^{-6}
β actin	gi|6671509	4.1	0.243	2.4×10^{-9}	12	54.40	22.87	1.3×10^{-23}
heat shock protein 9 (Hsc74)	gi|6754256	3.9	0.254	0.0011	4	21.06	8	1.0×10^{-8}
MAP/microtubule affinity-regulating kinase 4	gi|26986591	3.9	0.259	0.0067	1	6.91	2.09	0.0081
Predicted hypothetical protein similar to ribosomal protein L23	gi|149255181	3.8	0.264	9.6×10^{-5}	2	60.40	4.96	1.1×10^{-5}
Solute carrier family 25, member 4 (ADP/ATP translocase)	gi|148747424	3.7	0.274	0.0014	3	21.81	6.03	9.3×10^{-7}
Predicted protein similar to ribosomal protein L10-like	gi|82942312	3.3	0.300	0.0155	1	9.81	2.09	0.0081
Predicted hypothetical protein similar to ribosomal protein S5	gi|94404463	3.2	0.314	9.7×10^{-4}	4	35.84	8	1.0×10^{-8}
ribosomal protein S11	gi|21426889	3.2	0.317	4.8×10^{-4}	2	20.25	4.11	7.7×10^{-5}
Hypothetical ankyrin repeat containing protein LOC383787	gi|126517480	3.1	0.320	0.0209	2	11.79	4	1.0×10^{-4}
tubulin, beta 4	gi|31981939	3.1	0.320	0.0093	16	47.07	9.05	8.9×10^{-10}
Predicted hypothetical protein similar to ribosomal protein S13	gi|82919239	2.9	0.349	0.0049	2	19.21	4.55	2.8×10^{-5}
RAB11 family interacting protein 5, isoform 1	gi|52421788	2.8	0.352	0.0025	4	8.65	8	1.0×10^{-8}
ribosomal protein S9-like	gi|33504483	2.7	0.369	0.0066	3	19.07	5	1.0×10^{-5}
Predicted protein similar to histone H4	gi|94378251	2	0.501	0.0274	4	25.32	7.52	3.0×10^{-8}